Hindawi
Geofluids
Volume 2022, Article ID 8254114, 15 pages
https://doi.org/10.1155/2022/8254114

Research Article

Effect of Moisture on the Macro Failure Characteristics of Weakly Consolidated Mudstone: Mesomechanism

Jiahui Xu[1,2] **Guichen Li**[1,2] **Haoyu Rong**[1,2] **Mohamed Elgharib Gomah**[1,2] **Changlun Sun**[1,2] **Jinghua Li**[1,2] **and Suhui Zhang**[3]

[1]*Key Laboratory of Deep Coal Resource Mining, Ministry of Education of China, China University of Mining and Technology, Xuzhou 221116, China*
[2]*School of Mines, China University of Mining and Technology, Xuzhou 221116, China*
[3]*School of Civil Engineering, National Engineering Laboratory for High Speed Railway Construction, Central South University, Changsha 410075, China*

Correspondence should be addressed to Guichen Li; liguichen@cumt.edu.cn

Received 21 April 2022; Revised 29 May 2022; Accepted 6 June 2022; Published 1 July 2022

Academic Editor: Jim Shiau

Mudstone, whose significant characteristic is water-weakening, widely exists in all kinds of geotechnical engineering, which brings great security risks to engineering safety. In this paper, through a series of macro and meso test methods, the macro and meso action mechanism of water on the weakly consolidated plane of mudstone was studied. In the uniaxial compressive strength test, the mudstone cementation plane was the main part of the fracture derived. Under the moist state, the strength of mudstone would decrease significantly, which was inversely correlated with relative moisture content. In the case of flooding, mudstone cracking occurred only along the cementation plane. Through ESEM+mapping test, results showed the humidification curing caused obvious damage to the cemented plane, where sodium and calcium were lost without a certain cause. The cemented plane was rich in kinds of clay minerals in mesoscale and presented an inhomogeneous state. The surface hardness data obtained from nanoindentation were discrete and difficult to quantitatively evaluate the mesomechanical properties. However, compared with the dry state, the data set of the moist state had a significant decline, showing a weakening effect. The mudstone is prone to fail along these weakly consolidated planes. Moisture intrudes into the bedding plane further deteriorating their consolidation.

1. Introduction

The rock bolts would not be installed firmly when the anchorage is carried out in mudstone due to its characteristics of weakness and water-weakening, which results in a poor control effect. Mudstone widely exists in all kinds of geotechnical engineering, and the specific characteristics of various mudstones are different, which is mainly related to the key clay mineral components contained in them [1, 2]. To realize the stability control of mudrock mass, the physical and mechanical properties and weakening failure characteristics of mudrock mass should be clearly defined.

Under different environmental conditions, the physical properties of mudstone are obviously affected. Firstly, under the same humidity condition, the different internal pore sizes of mudstone are mainly affected by its types of minerals contained in them [3]. In the meantime, the internal pore's sizes of mudstone also affect their water holding capacity under different relative humidity conditions [4]. In addition, the porosity of mudstone will increase significantly during the process of humidification [5, 6] and the phenomenon of disintegration to different degrees occurs [7] under the dry-wet cycle. The creep displacement in the dry stage is relatively significant and accumulates with the progressive dry-wet cycle [8]. With the increase in the number of dry-wet cycles, the number of large particles decreases, while the number of small particles increases [9]. The structural characteristics and strength characteristics of the same kind of mudstone vary significantly with different moisture contents [10]. In addition, acidic liquid can relatively promote the disintegration of mudstone, while

an alkaline environment can relatively inhibit its disintegration [11, 12]. Laying polymer cement on the surface of mudstone can relatively inhibit the disintegration characteristics of mudstone when it meets water and temperature differences [13]. Its conductivity is also affected by pressure and temperature and is positively correlated with both [14].

At the same time, the mechanical properties and failure characteristics of mudstone show variability due to the different environments. Mudstone exhibits strain-softening characteristics under both wet-dry and wet-dry-freeze-thaw processes, and its failure strength decreases significantly [15]. Under freezing conditions, the uniaxial compressive strength of silty mudstone has a parabolic relationship with temperature [16]. The overall strength of mudstone is related to the expansion characteristics of mineral components and the internal cementation strength [17]. The higher the content of clay minerals, the smaller the uniaxial compressive strength and elastic modulus and the lower the cementation strength [18]. Under the coupled action of stress-seepage, the pore pressure increases first and then decreases with time, while the damaged area and permeability coefficient increase gradually and finally nearly keep constant [19]. In triaxial unloading experiments, specimens damaged under low initial unloading confining pressure usually have only a complete shear failure surface, while specimens damaged under high initial unloading confining pressure develop into tensile failure surface [20]. The increase of moisture content coefficient and temperature accelerates the creep deformation and creep strain rate of mudstone specimens [21], while the transverse creep characteristics of mudstone are more significant than the axial creep characteristics [22, 23]. Microscopic experiments based on the combination of acoustic emission (AE) and the digital speckle correlation method (DSCM) showed that sandy mudstone would produce serious microscopic damage during creep [24]. When the temperature is lower than 600°C, the uniaxial compressive strength of mudstone increases slowly with the increase of temperature [25]. At 600°C~800°C, the strength will slowly decline, reflecting the brittle-toughness transition characteristics [26]. Through the three-point bending test, it is clear that the brittle failure or ductile failure of mudstone is related to the stratification plane reflected by the specimen, and the anisotropy of mudstone will increase significantly under different moisture contents [27]. Under the action of high in situ stress and water-rock chemical interaction, wounds and fractures of damaged mudstone can heal themselves and restore their physical and mechanical properties [28]. Shear creep characteristics of fractured mudstone are related to axial pressure and fracture length. The larger the axial pressure is, the smaller the shear creep deformation is, while the longer the fracture is, the more obvious the shear creep deformation is [29]. Osmotic pressure will aggravate the rheological behavior and enhance the creep characteristics of mudstone, which are positively correlated [30]. Mudstone specimens with different buried depths show different strength characteristics, failure forms, and seepage characteristics. The shallow-buried mudstone has a higher compressive strength, which is mainly manifested as a brittle failure, while the buried mudstone at 1,000 m has a lower compressive strength, which is mainly characterized by ductile failure, but has relatively good permeability [31–33]. The hardness and elastic modulus of clay matrix and silt inclusion in mudstone were obtained through the nanoindentation test, and it was found that the elastic modulus of key mineral components was greater than that of mudstone itself [34].

Many scholars around the world have done a lot of research on mudstone. Combined with their research results, it can be found that the physical and mechanical properties of mudstone are correlated with its key mineral components, cementation properties, and environment. However, under the influence of water, there are few types of research on the internal relationship between the macroscopic mechanical properties of specific mudstone, its cementation structure, the types of clay minerals contained in it, and its mesoscopic mechanical properties, and the relevant mechanism needs to be clarified.

In this paper, a systematic study of mudstone is carried out by combining the uniaxial compressive strength (UCS) test at macroscale, environment scanning electron microscopy (ESEM+mapping) test, and nanoindentation technology at mesoscale, to reveal the interaction mechanism between the macroscopic failure characteristics of mudstone and its internal mesoscopic interaction of components.

2. Materials and Methods

2.1. Preparation for UCS Test. There were several mudstone specimens required for the experiment, all of which are standard cylinders in size of $\Phi \times L = 50 \times 100$ mm following the requirements of the International Rock Mechanics Association, and the flatness of the specimen end face is within 0.05 mm. Six specimens were taken from the collection, three of which were for the uniaxial compressive strength test and the other three were for the same thing but after humidification.

Quantitative control of moisture content of rock specimens was cumbersome and unnecessary. Therefore, the room temperature (RT = 21°C) and humidity conditions (RH = 93%) were controlled in the curing box for 24 h. After that, the size, weight, and relative moisture content were measured and the compressive strength was tested. Based on C64.106 electrohydraulic servo universal testing machine, the uniaxial compressive strength test was conducted with displacement control and a loading rate of 0.5 mm/min. In addition, to explore its water-physical property, small homologous mudstone rock specimens (1 cm cube) were processed and tested in Petri dishes.

2.2. Preparation for Mesoscopic Test. The water disturbance of mudstone directly led to its weakening, damage, and destruction, and it had different effects according to the different key mineral components contained in it. Therefore, the mudstone powder with homology to the standard rock specimen was processed and analyzed by a D8 Advance X-ray diffractometer after passing a 200-mesh screen, and the mineral components were quantified.

What is more, the conventional failure behavior of mudstone was closely related to its bond surface. Therefore, it was necessary to study and analyze the properties of the cementation plane of mudstone specimens. The apparent morphology and element distribution were characterized by

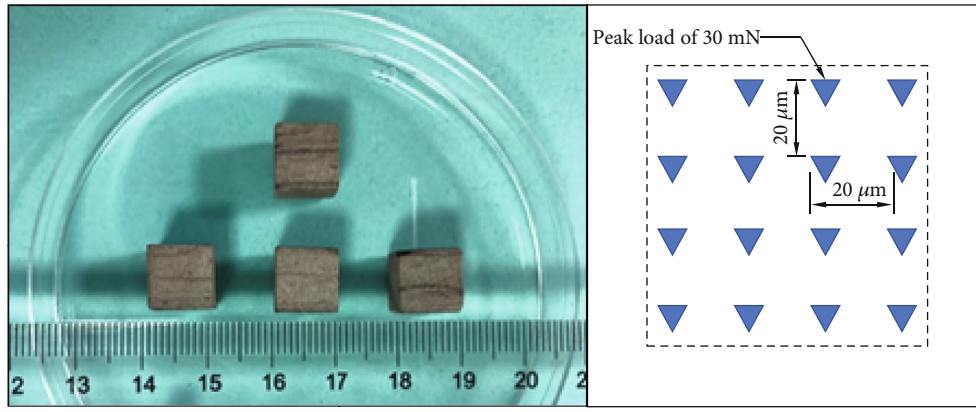

Figure 1: ESEM and nanoindentation specimen morphology and size with designed lattice form.

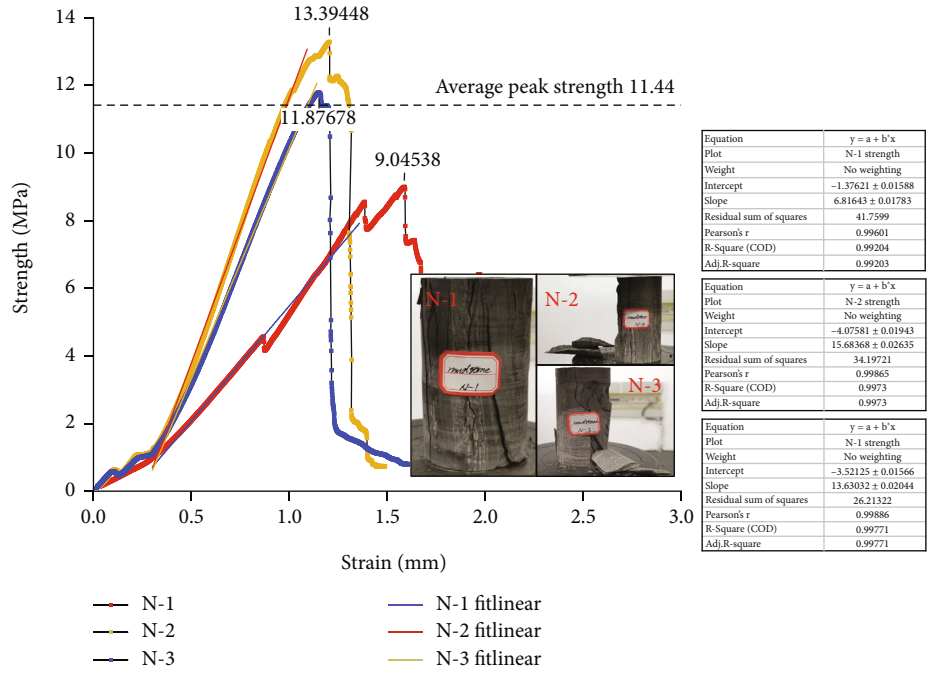

Figure 2: Failure modes and stress-strain curves of mudstone under the dry state.

ESEM+mapping. Based on Quanta 250 field emission scanning electron microscope, the mesostructure of the bond surface was obtained at 200x magnifications. The distribution characteristics of elements of the cementation plane were obtained by mapping energy spectrum analysis.

For the reason that it was difficult to conduct mechanical research on the weakly consolidated plane of mudstone specimens under the conventional experimental scale, nanoindentation technology was planned to be used to study it [35–37]. The specimens used in ESEM+mapping and nanoindentation experiments are shown in Figure 1, which was a 1 cm long cube homologous to the mudstone specimens used in the above-related experiments. Similarly, the surface of the specimen can be observed by the naked eye. The design lattice form was 4×4, the horizontal and longitudinal spacing between points was 20 μm, and a total of 16 points on one side occupied about 3,600 μm^2. The design point loading scheme was 30 mN.

3. Results of UCS Test and Mesoscopic Experiments

3.1. UCS and Failure Characteristics. The stress-strain curves and the corresponding failure modes of each specimen obtained from the test are shown in Figures 2 and 3.

No matter whether the mudstone specimen is in the dry state or the moist state, the initial stage of loading can present the elastic stage. The elastic modulus can be obtained by fitting the stress-strain curve in the elastic stage. After reaching the stress peak, all of them began to show one or more stress

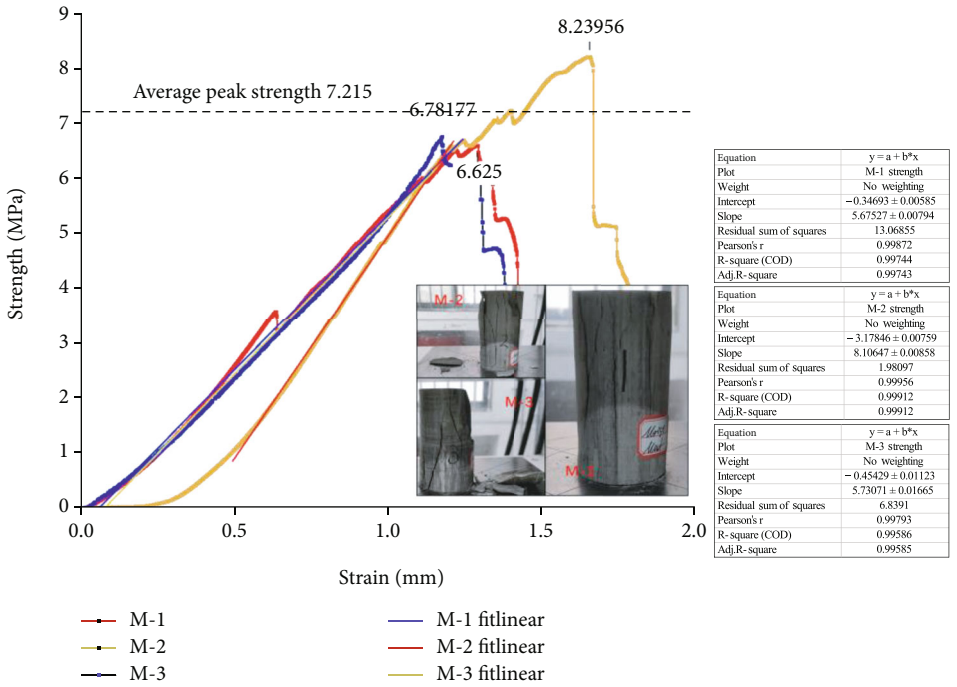

Figure 3: Failure modes and stress-strain curves of mudstone under the moist state.

Table 1: Basic test information of mudstone specimen before and after humidification curing.

Items	Dry				Moist							
	N-1	N-2	N-3	Average	M-1		M-2		M-3		Average	
					Before	After	Before	After	Before	After	Before	After
Length (mm)	100.13	100.12	99.94	100.06	100.36	100.37	100.33	100.33	100.38	100.4	100.36	100.36
Diameter (mm)	50.02	50.15	50.04	50.07	49.91	49.93	50.07	50.07	50.08	50.09	50.02	50.03
Weight (g)	400.25	404.17	410.23	404.88	391.15	396.12	418.72	423.58	406.23	411.18	405.37	410.29
RMC (%)	0	0	0	0	1.27		1.16		1.21		≈1.20	
UCS (MPa)	9.04	13.39	11.88	11.44	6.625		8.24		6.78		7.215	
E (GPa)	6.82	15.68	13.63	12.04	5.675		8.11		5.73		6.505	

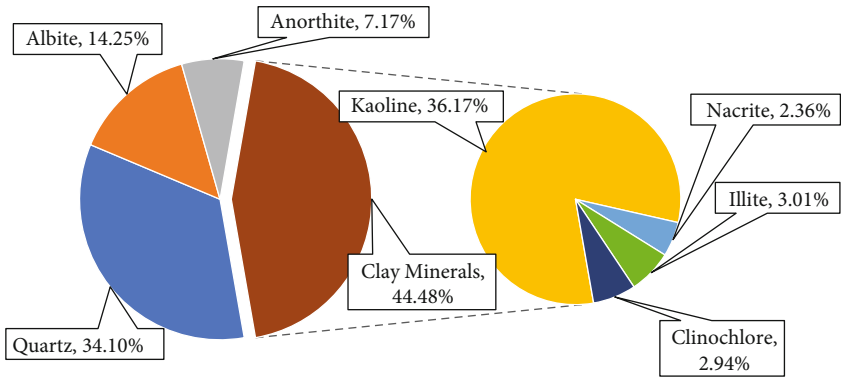

Figure 4: Types and contents of the main mineral components tested by XRD.

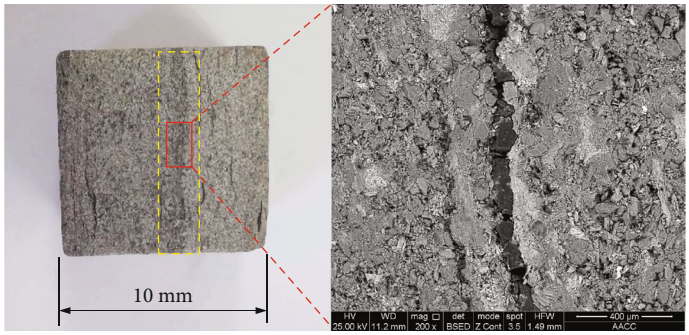

(a) The dry consolidated plane

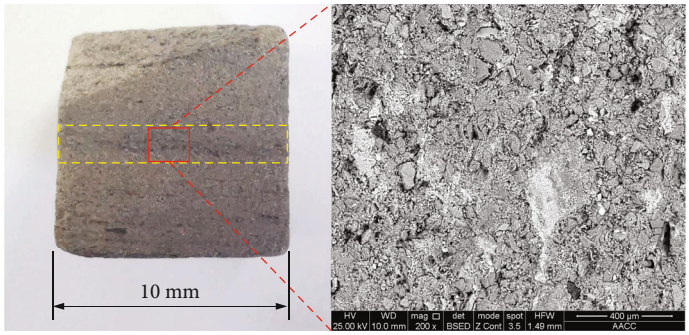

(b) The moist consolidated plane

Figure 5: Macro- and mesoscopic topography of consolidated plane before and after humidification.

drops. Each time the stress drop occurred, the cracks appeared synchronously. The specimens, whether in the dry state or moist state, are destroyed by compression which can be judged as a brittle splitting failure. The damage fissure was derived from the original heterogeneous stratified interface, and the damaged specimens appeared in lamellar form. The measurement and testing information of the specimen are summarized in Table 1.

After the UCS test of the three randomly selected mudstone specimens (relative moisture content – RMC = 0%), as shown in Table 1, average UCS and elastic modulus were about 11.44 MPa and 12.04 GPa, respectively, which are relatively low. After 24 h constant temperature and humidification curing, it was difficult to distinguish whether the rock specimen had an expansion phenomenon under the measurement error. However, the weight of specimens had increased significantly, whose measured relative moisture content was about 1.20%. The corresponding average UCS and elastic modulus are about 7.205 MPa and 7.76 GPa, respectively.

3.2. Mesostructure and Characteristic Elements. As shown in Figure 4, the main minerals were kaoline, quartz, and albite, with contents of 36.17%, 34.10%, and 14.25%, respectively. The main clay minerals occupied 44.48% that were kaoline, illite, nacrite, and clinochlore, of which kaoline occupies the highest proportion.

The morphology of the mudstone consolidated plane is shown in Figure 5 under macro- and mesoscale. At the macroscopic level, the stratified structure of the specimen surface could be easily distinguished by the naked eye. The interstratified boundary was clear, and the main color feature was black and white. At the same 200 magnification, the stratification structure was no longer visually visible, while it could be clearly identified that the matrix and particle were not homogeneous. After curing, the cracks between the particles were larger, the surface was relatively rough, and the apparent morphology was relatively loose.

Referring to Figure 6, the key elements were analyzed through ESEM+mapping, and it was found that O, Si, Fe, C, Al, K, Te, and Mg were the main 8 elements, both in weight percentage (wt %) and atomic percentage (at %). Among them, O, Si, Fe, C, and Al accounted for more than 90%. The quantitative results of major elements are shown in Table 2.

The measured surface topography, indentation distribution, and force-depth (Fn-Pd) curves of nanoindentation are shown in Figure 7. The test surface of the dry state was flat and smooth in the range of 60 μm wide, while the moist state was relatively rough, with distinct concave (dark) and convex (bright) surfaces that had a clear particles. For Fn-Pd curves, they appeared more uniform under the dry state, and the loading limit depth ranged from 427 nm to 3,560 nm under the peak stress condition of 30 mN. As for the moist state, the curves had obvious aggregation and dispersion characteristics. The loading limit depth at 1, 2, 4, 5, 8, and 9 points where were far from the particle was in the range of 6,000~15,000 nm which was discrete. The loading limit depth of the other points was between 1,420 and 3,720 nm which was relatively concentrated.

After fitting, the hardness and elastic modulus of each test point can be determined, as shown in Table 3.

After calculation and finishing, the test results of hardness and elastic modulus are shown in Table 3. In particular, the test results of point no. 3 of the dry state are abnormal. The elastic modulus (E) of the hardest component mineral, quartz, in the mudstone should be around 90 GPa [36], and

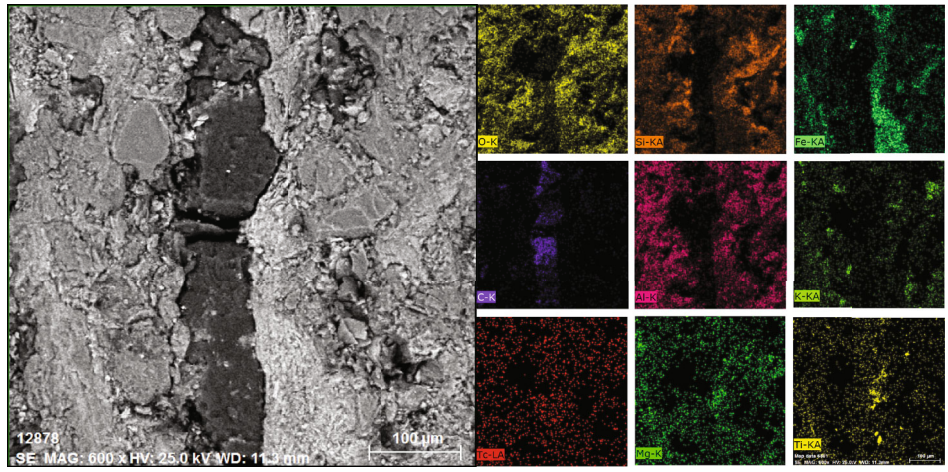

(a) In dry state

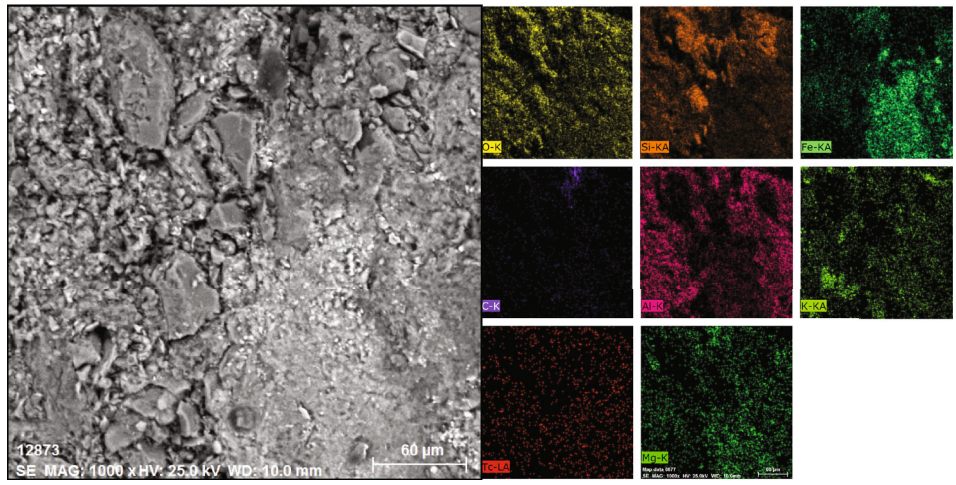

(b) In moist state

Figure 6: Mapping area and element distribution of mudstone in the dry state and moist state.

Table 2: Quantitative results of the main elements.

Element	Dry		Moist	
	wt%	at%	wt%	at%
Oxygen	47.18	52.18	47.29	55.38
Silicon	12.38	7.80	17.74	11.83
Iron	4.31	1.37	7.56	2.51
Carbon	20.40	30.06	13.25	20.67
Aluminum	9.31	6.10	10.84	7.52
Potassium	1.14	0.51	1.67	0.80
Technetium	0.04	0.01	0.02	0.00
Magnesium	1.06	0.77	1.63	0.25
Total	95.82	98.8	100	100

this data should not be taken into consideration. In the range of 60 μm × 60 μm, the hardness of the mudstone consolidated plane under the dry state ranged from 100 MPa to 3,870 MPa, and the E ranged from 4 GPa to 95 GPa. The hardness of mudstone after humidification curing was between 6 MPa and 800 MPa, and the elastic modulus was between 0.89 GPa and 17 GPa. No matter in the dry state or after humidification curing, the difference in mechanical properties of the consolidated plane was large and there was no obvious change rule. Thus, it was not suitable to use the mean value to express the hardness properties of the consolidated plane.

4. Analysis and Discussion of Mudstone Failure

4.1. The Macro Weakening Effect of Water. Through the analysis and comparison of Figure 8, it could be seen that the strength of mudstone specimens after humidification curing had obvious changes compared with the dry state.

Firstly, the uniaxial compressive strength of the mudstone after curing was obviously lower than that of the dry mudstone. In addition, the uniaxial compressive strength of mudstone had a certain correlation with its relative moisture content. The strength of mudstone could be reduced by 27.97%~42.09%, while elastic modulus was by 32.64%~52.865% when the relative moisture content was about 12.00‰. After humidification curing, the mudstone with higher relative moisture content had a higher strength loss rate. The weakening effect of water

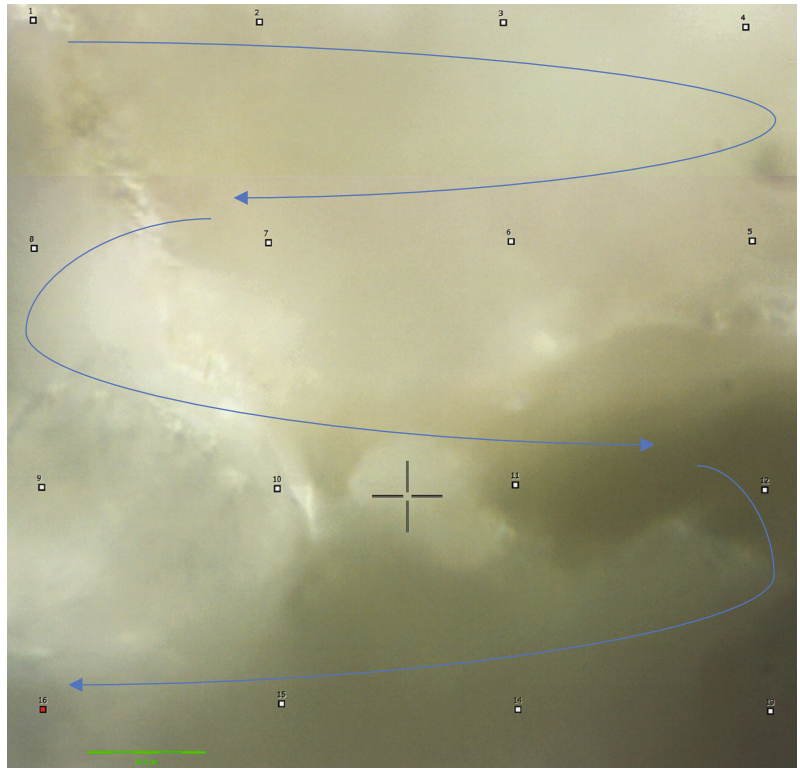

(a) Indentation distribution of the dry state

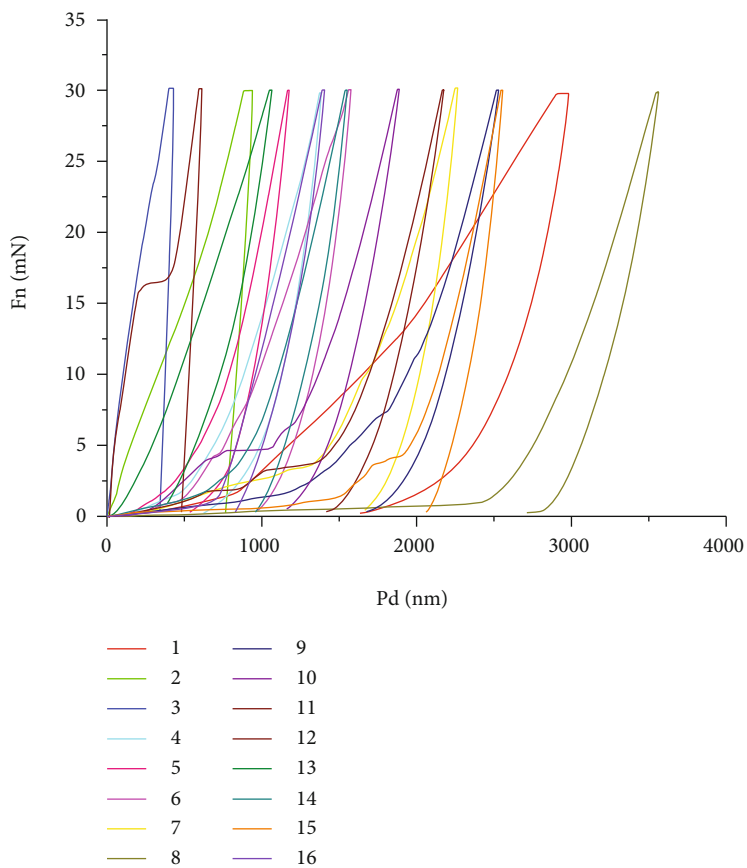

(b) Fn-Pd curves of the dry state

Figure 7: Continued.

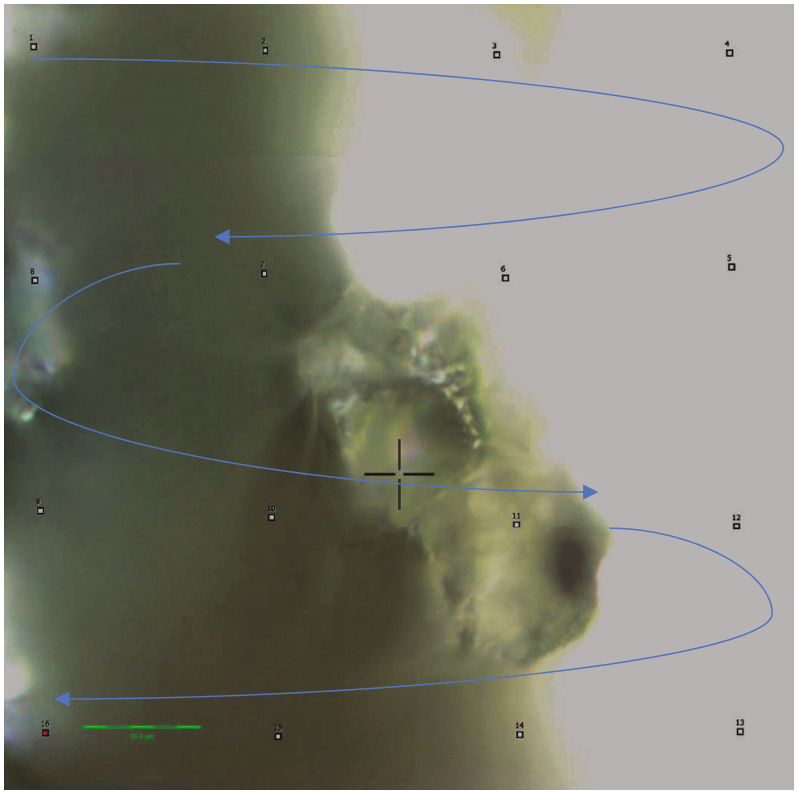

(c) Indentation distribution of the moist state

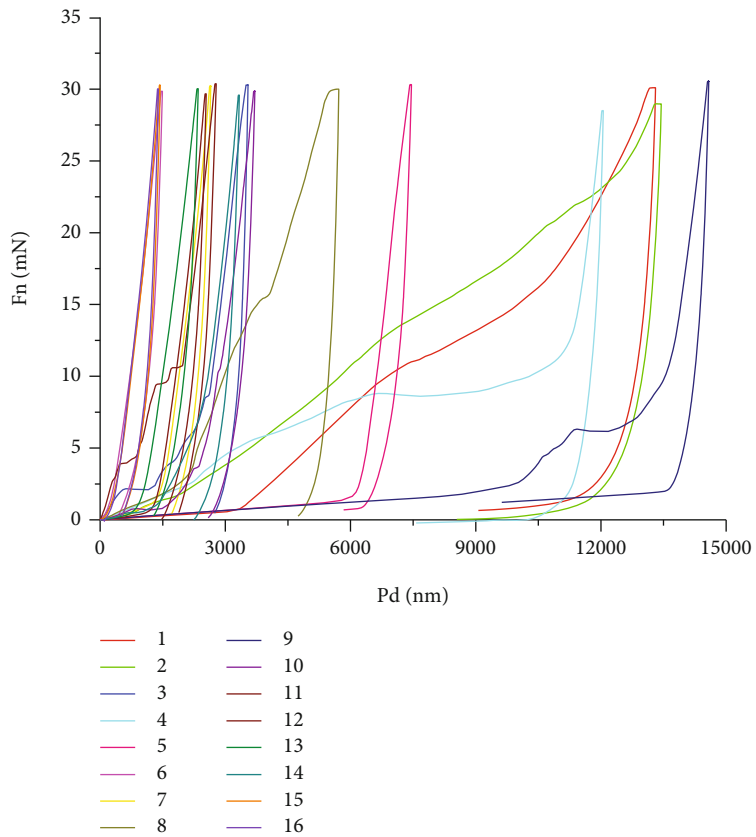

(d) Fn-Pd curves of the moist state

Figure 7: Indentation distribution and force-depth (Fn-Pd) curves of the dry and moist states.

Table 3: Surface hardness and elastic modulus (E) test results of the dry and moist states.

No.	Dry		Moist	
	Hardness (MPa)	E (GPa)	Hardness (MPa)	E (GPa)
1	161.03	5.0861	7.2043	0.93459
2	1590.3	48.877	6.791	0.89854
3	7111.6	259.54	105.24	7.6947
4	801.97	17.214	8.2267	1.418
5	1164	21.254	23.362	2.4301
6	598.16	15.559	710.32	13.864
7	273.3	10.542	199.42	8.0108
8	109.69	4.3567	39.15	4.1816
9	236.25	5.9223	6.0015	1.1958
10	450.37	8.7112	97.757	5.1411
11	326.02	7.4108	216.33	7.8022
12	3868.7	94.227	184.12	6.9577
13	1719.6	18.413	261.49	8.1908
14	638.11	14.33	119.85	6.1832
15	208.3	9.8534	755.26	15.946
16	799.3	15.913	794.01	16.979

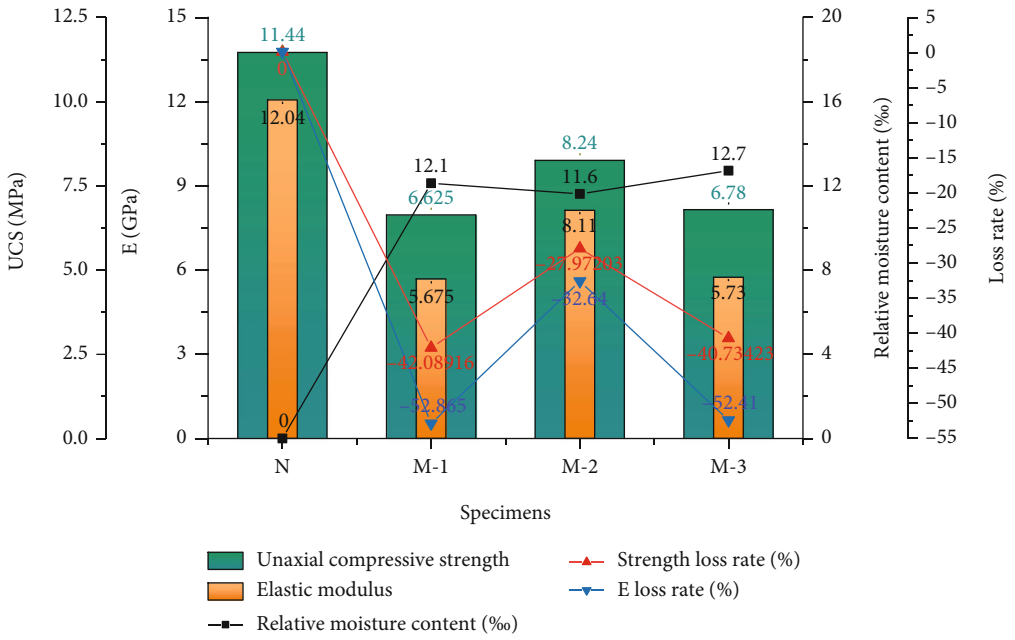

Figure 8: UCS and elastic modulus changes of mudstone after humidification.

on mudstone is significant. The weakening effect of water on the mudstone is mainly reflected in the damage to its cemented surface.

4.2. Cementation Morphology and Element Characterization. According to Figures 5 and 6, it had been clear that the mudstone cementation plane was also heterogeneous and was also composed of a variety of clay minerals mixed with other quartz, feldspar, and other mineral particles, which was susceptible to the influence of water [38]. In the dry state, the consolidated plane is where clay minerals (matrix state) are mixed with other mineral particles (particle state). The local matrix may be homogeneous and smooth, or it may be in a rough state with prominent particles. Nevertheless, two-dimensional surfaces do not tell the whole story in three-dimensional space. With other mineral particles buried beneath, a smooth clay matrix and only a small part of their volume exposed on the surface. After humidification, water invasions leaven or simply soften the clay matrix in a considerable area below the surface. This results in peeling off of

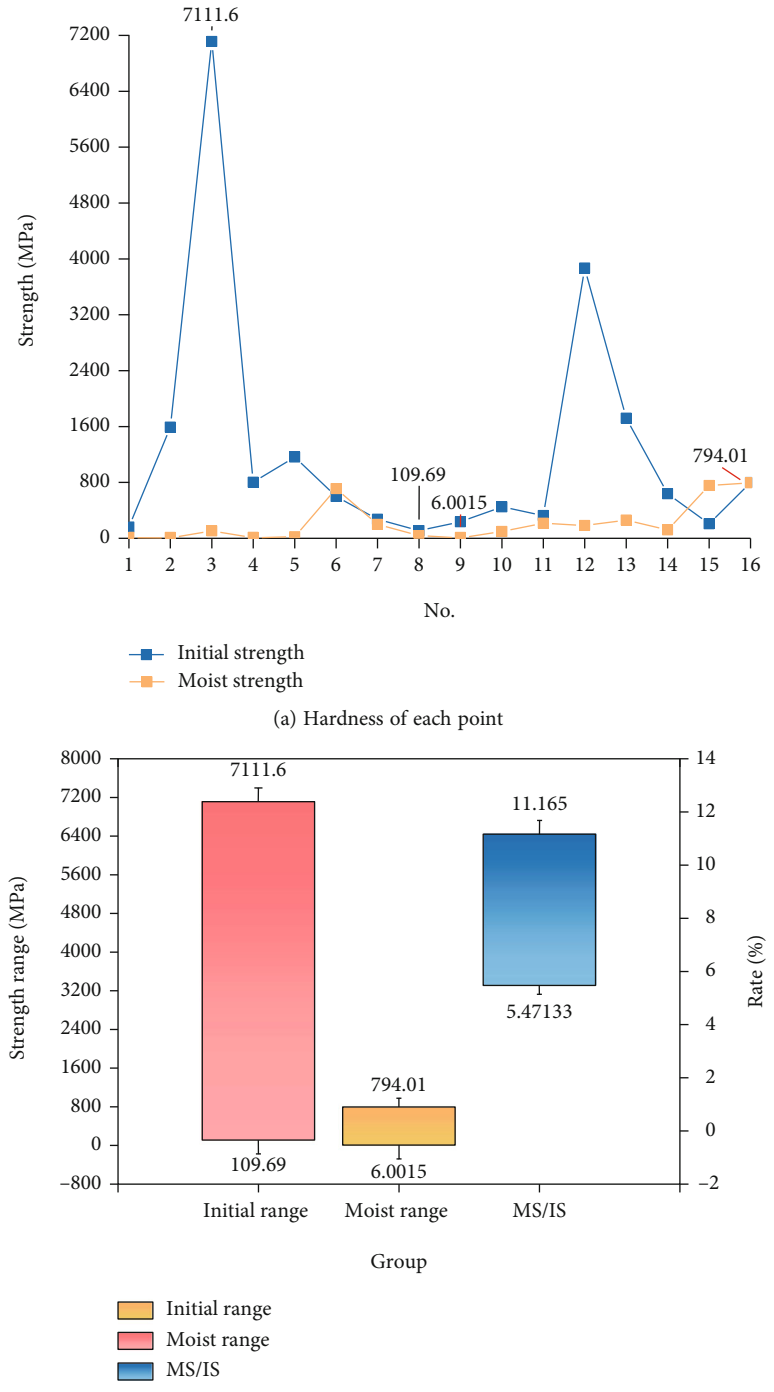

(a) Hardness of each point

(b) The hardness variety

Figure 9: Continued.

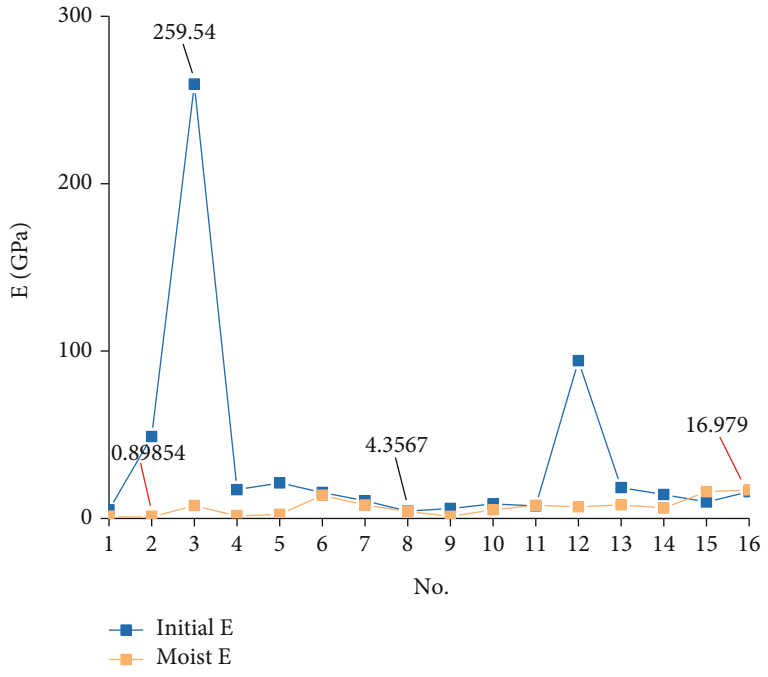

(c) Elastic modulus of each point

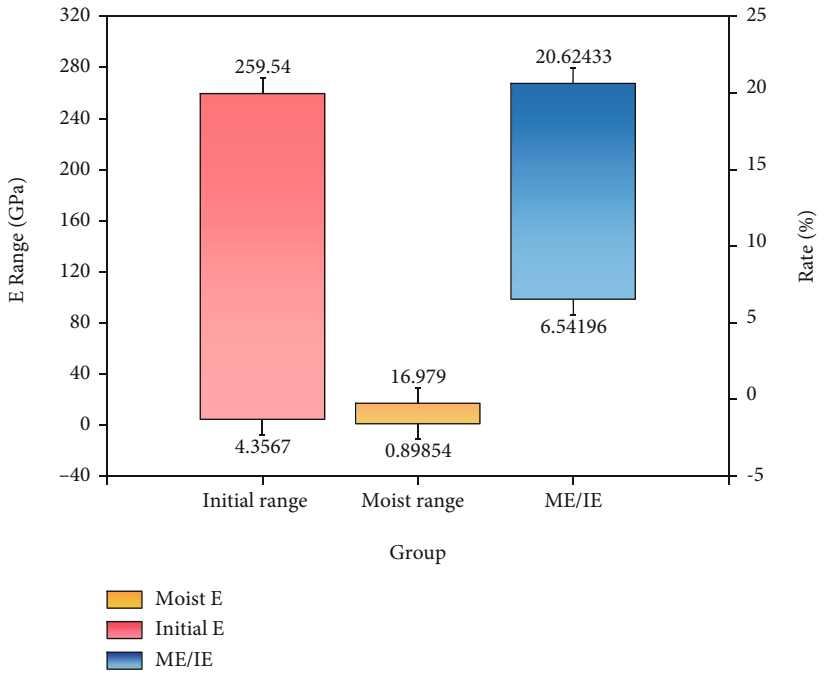

(d) The elastic modulus variety

Figure 9: The comparison of hardness and elastic modulus between the dry and the moist.

the clay matrix or the particles. After that, gullies and cracks occur on the weakly cemented plane at mesoscopic scales.

According to the distribution map of a single element, except for the obvious characteristics of element species and proportion, each element had different aggregation characteristics in the whole mapping area. Combined with the key mineral components obtained by the XRD test, it could be known that quartz (SiO_2), kaolin ($2SiO_2{\cdot}Al_2O_3{\cdot}2H_2O$), clinochlore ($Y3[Z_4O_{10}]{\cdot}(OH)_2{\cdot}Y_3(OH)_6$, Y for Mg or Fe; Z for Si or Al), albite ($Na_2O{\cdot}Al_2O_3{\cdot}6SiO_2$), illite ($KAl_2[(SiAl)_4O_{10}]{\cdot}(OH)_2{\cdot}nH_2O$), anorthite ($CaO{\cdot}Al_2O_3{\cdot}2SiO_2$), and nacrite ($2SiO_2{\cdot}Al_2O_3{\cdot}2H_2O$) were contained in mudstone.

According to the molecular formula and the main elements of the main mineral components, combined with Table 2, it can be seen that O and Si elements were presented in every mineral; even though they had the highest abundance, they did not have the function of representing specific mineral

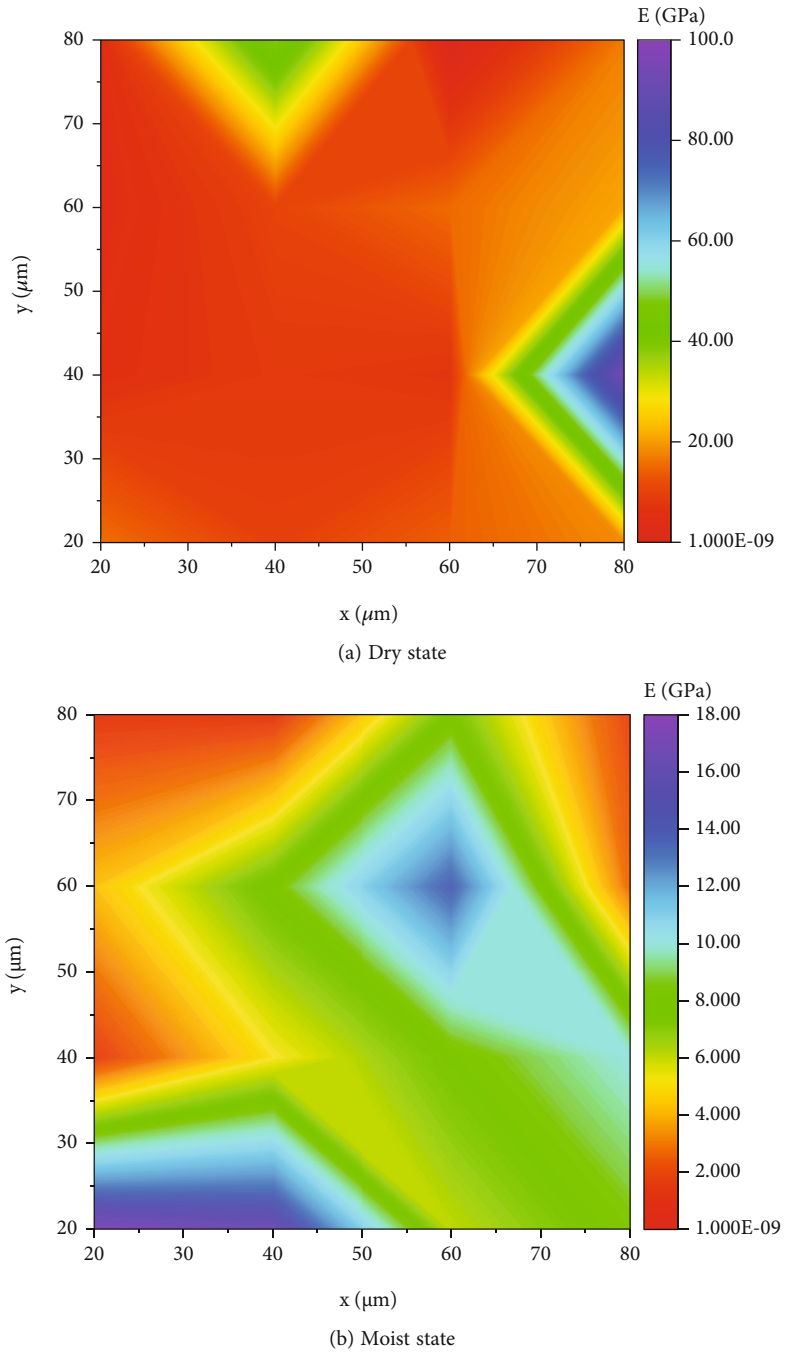

Figure 10: Contour of surface elastic modulus variation of the dry and the moist states.

components. Several metal elements, such as Na, K, and Ca, which could effectively represent specific minerals, were processed by element stacking. It should be noted that Na and Ca elements were not detected on the mapping surface in the moist state, which was different from the distribution of Na and Ca elements along with the matrix and particles in the dry state. That was most likely because it migrated with surface moisture in the ion state during humidification curing, resulting in the loss of superficial related elements. The distribution of aluminum in the dry state was basically within the range of the matrix, and the distribution of aluminum in the humidified state was also uneven, which can basically cover all kinds of clay minerals except quartz. K, Mg, and Fe elements had unique distribution characteristics, which were scattered and interfered with each other. The area not covered by those parts of metal elements can be considered the main distribution area of quartz. Thus, it is clear that the obvious bedding observed at the macro level is still composed of quartz mixing with many clay minerals at the mesoscopic level.

4.3. Mesomechanical Properties of Mudstone Cementation. As shown in Figure 9, the data obtained from the nanoindentation test fluctuates widely with a significant difference. However, it is obvious that although the hardness

characteristics are not very clear either in the dry state or after humidification curing, the hardness and elastic modulus of the cemented interface of mudstone after humidification curing is much lower than that in the dry state. The lower limit of hardness is about 5.47% of the dry state, and the upper limit is about 11.165%. The lower limit of elastic modulus is about 20.62% of the dry state and is 6.54% of the upper limit. After humidification, water had an obvious weakening effect on the mechanical properties of the consolidated plane.

As shown in Figure 10, the surface elastic modulus of the specimen in the dry state and the moist state has a certain correlation with the test surface morphology, but it is not completely consistent. Relatively smooth and uniform plane A (dry state) presents low elastic modulus, while abnormal high elastic modulus exists in local positions. In rough plane B (moist state), the elastic modulus near the particle is obviously higher, but there is a certain range of high values in the convex and concave parts.

As for the mesomechanical properties of a weakly cemented plane, the main difference is the softening of the matrix. When the nanoprobe is pressed at a certain depth, it encounters mineral particles that are shallow below the clay matrix of the surface, or when the probe is pressed on the surface, the clay matrix below the particle is softened by wetting and can be pressed deeper with relative ease. Thus, the smooth and uniform test surface showed abnormally high values, and the concave and convex surfaces except the particles showed a phenomenon of high elastic modulus.

As for the macroscopic mechanical properties, the influence of meso- or microgullies and cracks resulting from the softening of the clay matrix plays the main role. Under the macrocompressive loading, the whole specimen starts to hold the force. There are meso- or microgullies and cracks that exist in the mudstone; these places are more prone to stress concentration compared to other parts which are relatively smooth. Meanwhile, the subtle damages were happening all the time during the compression process, the accumulation of which leads to the connection of gullies and cracks and their expansion on the surface and inside. Eventually, the broken specimen shows the cracks derive along the weakly cemented plane.

5. Conclusion

This study investigated the mesoscopic effect of water on the consolidated plane of mudstone under moist conditions, as well as the linkage mechanism between the macro failure modes caused by water in detail through a variety of macro and micro test methods, such as UCS, XRD, ESEM+mapping, and nanoindentation technology. The following conclusions are drawn:

(1) The bedding bond plane of mudstone is the weak part causing failure under stress conditions. For mudstone with an obvious bedding structure, when the loading direction of compression is parallel to the stratification of the specimen, the crack generated by the specimen failure basically derives along the cementation plane

(2) Water has a significant weakening effect on mudstone specimens, especially on the bedding bond surface. The wetting condition weakens the uniaxial compressive strength of mudstone obviously compared with the dry condition

(3) The weakly consolidated surface of mesoscopic mudstone is still rich in clay minerals. The macroscopic clear and distinguishable cementation plane is no longer visible at the mesoscale, but the cementation plane is still a mixture of various clay minerals (matrix state) and quartz, feldspar, etc. (particle state). Na and Ca elements are lost in the humidification curing process of mudstone specimens

(4) Water has obvious damage to the consolidated plane of mudstone at the mesoscopic level. The shape of the consolidated plane after wetting is different from that of the original state, but it is relatively rough, and the surface cracks and particles are obvious

(5) The mechanical properties of weakly consolidated mudstone are determined by the nature of its weakly consolidated plane. The mesomechanical properties are mainly affected by water and the composition of clay matrix and fine mineral particles. The former leads to the decline of the overall performance, while the latter causes the dispersion of its surface strength. The macromechanical properties are mainly affected by the stress concentration caused by the meso or micro damages caused by the softening and spalling of the clay matrix on the weakly consolidated plane

Data Availability

The data used to support the findings of this study are available from the corresponding author upon request.

Conflicts of Interest

The authors declare that they have no known competing financial interests or personal relationships that could have appeared to influence the work reported in this paper.

Acknowledgments

The authors gratefully acknowledge the financial support from the National Natural Science Foundation of China (No. 52174089), the Postgraduate Research & Practice Innovation Program of Jiangsu Province (No. KYCX22_2614), the Fundamental Research Funds for the Central Universities (No. 2020ZDPY0221), and the Assistance Program for Future Outstanding Talents of China University of Mining and Technology (No. 2022WLKXJ043).

References

[1] N. H. Koralegedara and J. B. Maynard, "Chemical, mineralogical and textural properties of the Kope Formation mudstones: how they affect its durability," *Engineering Geology*, vol. 228, pp. 312–322, 2017.

[2] Z. Doner, Q. Hu, M. Kumral, M. G. Kibria, H. Qiao, and M. Sun, "Petrophysical characteristics of Silurian mudstones from central taurides in southern Turkey," *Journal of Earth Science*, vol. 32, no. 4, pp. 778–798, 2021.

[3] Y. Qi, Y. Ju, C. Huang et al., "Influences of organic matter and kaolinite on pore structures of transitional organic-rich mudstone with an emphasis on S_2 controlling specific surface area," *Fuel*, vol. 237, pp. 860–873, 2019.

[4] X. Niu, Y. Han, G. Feng, and J. Cui, "Effect of the physicochemical structure of mudstone on readsorption behavior of water," *Energy & Fuels*, vol. 35, no. 1, pp. 386–396, 2021.

[5] Y. Zhao, S. Ren, D. Jiang, R. Liu, J. Wu, and X. Jiang, "Influence of wetting-drying cycles on the pore structure and mechanical properties of mudstone from Simian Mountain," *Construction and Building Materials*, vol. 191, pp. 923–931, 2018.

[6] M. Hu, Y. Liu, J. Ren, R. Wu, and Y. Zhang, "Laboratory test on crack development in mudstone under the action of dry-wet cycles," *Bulletin of Engineering Geology and the Environment*, vol. 78, no. 1, pp. 543–556, 2019.

[7] W. Liu and Z.-h. Zhang, "Experimental characterization and quantitative evaluation of slaking for strongly weathered mudstone under cyclic wetting-drying condition," *Arabian Journal of Geosciences*, vol. 13, no. 2, 2020.

[8] K. Sharma, T. Kiyota, and H. Kyokawa, "Effect of slaking on direct shear behaviour of crushed mudstones," *Soils and Foundations*, vol. 57, no. 2, pp. 288–300, 2017.

[9] L. Zeng, J.-T. Luo, J. Liu, Q.-F. Gao, and H.-B. Bian, "Disintegration characteristics and mechanisms of carbonaceous mudstone subjected to load and cyclic drying-wetting," *Journal of Materials in Civil Engineering*, vol. 33, no. 8, 2021.

[10] Z. Wang, J. Du, S. Wu et al., "Water softening mechanism and strength model for saturated carbonaceous mudstone in Panzhihua Airport, China," *Advances in Civil Engineering*, vol. 2020, Article ID 8874201, 12 pages, 2020.

[11] X. Su, H. Tang, L. Huang, P. Shen, and D. Xia, "The role of pH in red-stratum mudstone disintegration in the Three Gorges reservoir area, China, and the associated micromechanisms," *Engineering Geology*, vol. 279, p. 105873, 2020.

[12] X. Chen, H. Yi, L. Gao, X. Shi, and Y. Liu, "Effects of inhibitor KCl on hydration swelling and softening of a smectite-poor mudstone," *Journal of Petroleum Exploration and Production Technology*, vol. 10, no. 7, pp. 2685–2692, 2020.

[13] X. Liu, Y. Li, S. Li, and Y. Zhou, "Research on the disintegration characteristics of carbonaceous mudstone and properties of modified materials," *Advances in Civil Engineering*, vol. 2019, 10 pages, 2019.

[14] W. Sun, L. Dai, H. Li, H. Hu, L. Wu, and J. Jiang, "Electrical conductivity of mudstone (before and after dehydration at high P-T) and a test of high conductivity layers in the crust," *American Mineralogist*, vol. 102, no. 12, pp. 2450–2456, 2017.

[15] R. Zhu, Y.-h. Huang, Z. Song, and F. Zhou, "Volume changes and mechanical properties of expansive mudstone below canals under wet-dry/wet-dry-freeze-thaw cycles," *Advances in Civil Engineering*, vol. 2021, 11 pages, 2021.

[16] L. Liu, X. Liu, Z. Li, Z. Yao, and G. Cai, "Experimental analysis on the mechanical properties of saturated silty mudstone under frozen conditions," *Journal of Testing and Evaluation*, vol. 47, no. 1, pp. 20170080–20170202, 2019.

[17] J. Liu, Q. Zhang, F. Chen, and T. Li, "Study on expansion mechanism of mudstone under structural strength," in *3rd International Workshop on Renewable Energy and Development (IWRED); 2019*, Guangzhou, Peoples R China, 2019.

[18] G. Li, C. Sun, J. He, Y. Sun, Y. Dong, and H. Zhao, "Macro and meso scale simulation study of the strength-weakening property of soft mudstone affected by water," *Zhongguo Kuangye Daxue Xuebao/Journal of China University of Mining and Technology*, vol. 48, pp. 935–942, 2019.

[19] B. Liu, J. Li, Q. Liu, and X. Liu, "Analysis of damage and permeability evolution for mudstone material under coupled stress-seepage," *Materials*, vol. 13, no. 17, p. 3755, 2020.

[20] X. Yuan, "Study on strength and deformation characteristics of sandy mudstone based on triaxial unloading test," in *3rd International Conference on Energy Materials and Environment Engineering (ICEMEE); 2017*, Bangkok, Thailand, 2017.

[21] Y. Lu and L. Wang, "Effect of water and temperature on short-term and creep mechanical behaviors of coal measures mudstone," *Environmental Earth Sciences*, vol. 76, no. 17, 2017.

[22] H. C. Yu, H. D. Liu, Z. Q. Huang, and G. C. Shi, "Experimental study on time-dependent behavior of silty mudstone from the Three Gorges Reservoir Area, China," *KSCE Journal of Civil Engineering*, vol. 21, no. 3, pp. 715–724, 2017.

[23] Q. Wang, X. Hu, C. Xu, C. Zhou, C. He, and C. Ying, "Time-dependent behavior of saturated silty mudstone under different confining pressures," *Bulletin of Engineering Geology and the Environment*, vol. 79, no. 5, pp. 2621–2634, 2020.

[24] H. Jing, Q. Yin, S. Yang, and W. Chen, "Micro-mesoscopic creep damage evolution and failure mechanism of sandy mudstone," *International Journal of Geomechanics*, vol. 21, no. 3, 2021.

[25] Q. Wang, Y. Zhang, X. Wang, L. Chen, and X. Zhang, "Experimental study on mechanical behaviors of mudstone under real-time temperature," in *3rd International Workshop on Advances in Energy Science and Environment Engineering (AESEE); 2019*, Suzhou, Peoples R China, 2019.

[26] L. Zhang, X. Mao, M. Li, B. Li, R. Liu, and A. Lu, "Brittle-ductile transition of mudstone in coal measure rock strata under high temperature," *International Journal of Geomechanics*, vol. 20, no. 1, 2020.

[27] J. Yang, L. Li, and H. Lian, "Experimental investigation of the effects of water content on the anisotropy of mode I fracture toughness of bedded mudstones," *PLoS One*, vol. 15, no. 8, 2020.

[28] J. Xu, J. Qu, Y. Gao, and N. Xu, "Study on the elastoplastic damage-healing coupled constitutive model of mudstone," *Mathematical Problems in Engineering*, vol. 2017, 7 pages, 2017.

[29] L. Z. Wu, S. H. Li, P. Sun, R. Q. Huang, and B. Li, "Shear creep tests on fissured mudstone and an improved time-dependent model," *Pure and Applied Geophysics*, vol. 176, no. 11, pp. 4797–4808, 2019.

[30] C. Ma, T. Zhang, and W. Yao, "An assessment of the osmotic pressure effect on the creep properties of silty mudstone," *Soil Mechanics and Foundation Engineering*, vol. 56, no. 5, pp. 314–320, 2019.

[31] T. Xin, Y. Sun, J. Wang, and W. Sun, "Influence of unloading conditions of confining pressure on the compressive strength and permeability of deep mudstone," *Advances in Civil Engineering*, vol. 2021, 10 pages, 2021.

[32] J. Jia, F. Yu, Y. Tan, and X. Gao, "Experimental investigations on rheological properties of mudstone in kilometer-deep mine," *Advances in Civil Engineering*, vol. 2021, 12 pages, 2021.

[33] U. C. Iyare, O. O. Blake, and R. Ramsook, "Modelling the failure behaviour of mudstones under high pressures," *Rock Mechanics and Rock Engineering*, vol. 54, no. 6, pp. 2815–2828, 2021.

[34] C. Sun, G. Li, M. E. Gomah, J. Xu, and H. Rong, "Meso-scale mechanical properties of mudstone investigated by nanoindentation," *Engineering Fracture Mechanics*, vol. 238, p. 107245, 2020.

[35] C. L. Sun, G. C. Li, M. E. Gomah, J. H. Xu, and Y. T. Sun, "Creep characteristics of coal and rock investigated by nanoindentation," *International Journal of Mining Science and Technology*, vol. 30, no. 6, pp. 769–776, 2020.

[36] C. Sun, G. Li, J. Xu, H. Rong, and Y. Sun, "Rheological characteristics of mineral components in sandstone based on nanoindentation," *Yanshilixue Yu Gongcheng Xuebao/Chinese Journal of Rock Mechanics and Engineering*, vol. 40, pp. 77–87, 2021.

[37] C. Sun, G. Li, M. E. Gomah, J. Xu, and H. Rong, "Experimental investigation on the mechanical properties of crushed coal samples based on the nanoindentation technique," *Meitan Xuebao/Journal of the China Coal Society*, vol. 45, pp. 682–691, 2020.

[38] J. Du, L. Hu, J. N. Meegoda, and G. Zhang, "Shale softening: observations, phenomenological behavior, and mechanisms," *Applied Clay Science*, vol. 161, pp. 290–300, 2018.